This is a preprint, the final version is subject to change, of the American Mineralogist (MSA)
Cite as Authors (Year) Title. American Mineralogist, in press.
(DOI will not work until issue is live.) DOI: http://dx.doi.org/10.2138/am.2013.4485

Revision 1

Mechanism of mineral transformations in krennerite, Au_3AgTe_8, under hydrothermal conditions

Weina Xu[1,2], Jing Zhao[2,3], Joël Brugger[2,4], Guorong Chen[1], and Allan Pring[2,5*]

[1] Key Laboratory for Ultrafine Materials of Ministry of Education, School of Materials Science and Engineering, East China University of Science and Technology, Shanghai 200237, China

[2]Department of Mineralogy, South Australian Museum, North Terrace, Adelaide, SA 5000, Australia

[3]School of Chemical Engineering, University of Adelaide, Adelaide, SA 5005, Australia

[4]Tectonics, Resources and Exploration (TRaX), School of Earth and Environmental Sciences, University of Adelaide, Adelaide, SA 5005, Australia

[5] School of Chemistry and Physics Sciences, University of Adelaide, Adelaide, SA 5005, Australia

*Corresponding author: allan.pring@samuseum.sa.gov.au

Abstract

Calaverite, krennerite and sylvanite are Au-Ag-tellurides with close compositions and related crystal structures. Previous experimental studies show that both calaverite and sylvanite transform to porous 'mustard' gold under hydrothermal conditions; however the transformation of sylvanite follows a complex reaction path with a number of intermediary products, contrasting with the simple replacement of calaverite by gold. Here we report results of an experimental study of the transformation of krennerite, a phase with Ag contents intermediate between those of calaverite and sylvanite.

Krennerite was replaced by Au-Ag alloy under all experimental conditions explored (160 to 220 °C; pH_T ~ 3 and 9; varying availability of oxygen). No reaction was observed at the same temperature under dry conditions. The replacement was pseudomorphic and the resulting Au-Ag alloy was porous, consisting of worm-like aggregates with diameters ranging from 200 nm to 1 μm. The replacement of krennerite proceeds via an interface coupled dissolution-(re)precipitation (ICDR) reaction mechanism. Tellurium is lost to the bulk solution as Te(IV) complexes, and may precipitate away from the dissolution site. In contrast, Au-Ag alloy precipitates locally near the krennerite dissolution site. Overall, the hydrothermal alteration of krennerite is very similar to that of calaverite, but differs from the alteration of sylvanite, for which multi-step reaction paths led to complex products and textures under similar conditions. These striking differences are driven by the competition between solid-state reactions and ICDR reaction in sylvanite. This reflects the fact that a metastable, Ag-rich calaverite nucleates on sylvanite during the early steps of its dissolution, as a result of the close relationship between the structures of these two minerals and the enrichment in Au, Ag and Te in solution at the reaction front. In contrast, for calaverite and krennerite, no such phase precipitates, and both minerals are transformed in a pseudomorphic manner into Au-Ag alloy.

Keywords: krennerite, gold, dissolution-reprecipitation, pseudomorphism, replacement.

Introduction

Gold silver tellurides are important accessory minerals in many Au deposits (Cook et al. 2009), and carry a significant proportion of the Au in deposits such as the Golden Mile, Kalgoorlie, Australia (Shackleton and Spry 2003) and Emperor, Fiji (Ahmad et al. 1987). Common Au-Ag-tellurides including calaverite, sylvanite and petzite are found in both low-temperature hydrothermal veins (≤200 °C) and moderate- to high-temperature (>450 °C) deposits (Cabri 1965).

Zhao et al. (2009, 2010, 2013) studied the reactivity of calaverite and sylvanite at temperatures above 200 °C over a wide range of hydrothermal conditions. Calaverite and sylvanite can have overlapping compositions, and share a similar layer structure topology (Figs. 1 and 2). Under oxidizing conditions Te was lost to the bulk solution as Te^{4+} complexes (Zhao et al. 2009, 2010 and 2013). Ultimately, calaverite and sylvanite are replaced in a pseudomorphic manner by high porosity gold or Au-Ag alloy, which form worm-like aggregates with diameters ranging from 200 nm to 1 μm. In the replacement of calaverite by gold (Zhao et al. 2009, 2010), the transformation proceeds in a pseudomorphic manner via an Interface Coupled calaverite Dissolution-gold (Re)precipitation (ICDR) mechanism, with calaverite dissolution being rate-limiting relative to gold precipitation. The porous gold obtained under hydrothermal conditions in Zhao et al. (2009)'s study is reminiscent of natural mustard gold, implying that natural mustard gold, which results from the weathering of Au-tellurides, may form via a similar dissolution-reprecipitation mechanism.

In contrast, the transformation of sylvanite to Au-Ag alloy follows a complex reaction path, and results in complex textures. In addition to Au-Ag alloy, a range of other phases form as intermediate products, including petzite (Ag_3AuTe_2), hessite (Ag_2Te), and two compositions

of calaverite: an Ag-rich-Te depleted composition, $(Au_{0.78}Ag_{0.22})Te_{1.74}$, and a normal calaverite, $(Au_{0.93}Ag_{0.07})Te_2$. This complexity is due to the fact that ICDR reactions compete with solid state reactions in sylvanite (Zhao et al. 2013). Initially, sylvanite was replaced by Au-Ag alloy following an ICDR mechanism. Tellurium was lost to the bulk solution as tellurite (oxidizing conditions; Grundler et al. 2013) or polytelluride (reducing conditions; Brugger et al. 2012) complexes. Once the concentration of Te in solution reached a critical state, the reaction switched and sylvanite dissolution was coupled to precipitation of an Ag-rich-Te-depleted calaverite. This Ag-rich-Te-depleted calaverite broke down via exsolution to calaverite and phase *X* ($Ag_{3+x}Au_{1-x}Te_2$ with $0.1 < x < 0.55$), which in turn broke down to a mixture of low petzite and low hessite below 120 °C via exsolution. As the reaction continues, the calaverite and phase *X* are all transformed to Au-Ag alloy via ICDR.

To further track the fate of Ag during the transformation and to investigate the effect of Ag in the parent crystal for the reaction path of Au-Ag-tellurides, we designed a set of hydrothermal experiments using krennerite. The krennerite from the Kalgoorlie deposit used in these experiments has Ag contents between those of the Kalgoolie calaverite used by Zhao et al. (2009, 2010) and the Emperor sylvanite used by Zhao et al. (2013) (Fig. 1). In first approximation, calaverite and sylvanite share a topographically similar layered structure; in contrast, the structure of krennerite can be described as calaverite with ordered twin m-mirror planes leading to orthorhombic symmetry (Dye and Smyth 2012), and resulting in a 'zig-zag' pattern (Fig. 2).

Here we present the results of a laboratory study into the transformation of krennerite to gold (or an Au-Ag alloy) over a range of hydrothermal conditions. This work aims to establish the mechanism of mineral replacement of krennerite, to characterize the resulting textures, and to compare these results to our previous studies on the replacement of calaverite and sylvanite (Zhao et al. 2009, 2010 and 2013).

Samples and methods

Composition and preparation of natural krennerite

Krennerite crystals were sourced from the Golden Mile, Kalgoorlie, Western Australia (SA Museum specimen G28219). The identification of the krennerite was confirmed by X-ray powder diffraction (XRD). Electron probe microanalysis based on 30 points gave [mean, (range), as wt%]: Te 59.1 (58.2–60.1); Au 37.4 (36.3–38.8); Ag 4.6 (4.3–4.8); Sb 0.39 (0.35–0.45); total 101.4. The resulting average formula for krennerite is $Au_{3.28}Ag_{0.72}Sb_{0.06}Te_{8.00}$ (Au:Ag = 4.6), close to the revised formula Au_3AgTe_8 recently proposed by Dye and Smyth (2012) on the basis of a high quality crystal structure refinement on a crystal from the Little Clara Mine in the Cripple Creek District, Colorado. The krennerite from Kalgoorlie is richer in Au than that from Cripple Creek ($Au_{2.87\text{-}2.97}Ag_{0.85\text{-}0.94}Te_8$, based on 7 points; Au:Ag = 3.1-3.5; Dye and Smyth, 2012). Two krennerite crystals from the Moose and Vindicator Mines at Cripple Creek analyzed by Tunell and Murata (1950) also had lower Au:Ag ratios than that of Kalgoorlie (Au:Ag ratios of 4.07 and 3.56). For the hydrothermal experiments, hand-picked krennerite was ultrasonically washed in deionized water, crushed and sieved into the size fraction of 125-150 μm.

Preparation of buffer solutions

To study the effect of pH on the reaction mechanism, two buffer solutions of $pH_{25°C} \sim 2$ (P2) and ~ 10 (B10) were prepared using Milli-Q water (conductivity of 18 MΩ cm^{-1}; Direct Q3 system, Millipore corp.). The phosphate buffer solution (P2) was prepared using 0.1044 *m* H_3PO_4 and 0.0954 *m* NaH_2PO_4, while B10 was a borate buffer solution with the composition of 0.1064 *m* H_3BO_4 and 0.1820 *m* NaOH. A small quantity of chloride (0.01 *m* NaCl) was added; this was enough to act as a ligand for Au and Ag, but low enough to prevent precipitation of AgCl(s). pH measurements were performed at room temperature using a temperature-corrected pH-meter (EUTECH Scientific, model Cyber-scan 510) with an

Ag/AgCl pH electrode. Calibrations were carried out using AQUASPEX standard buffer solutions: KH-phthalate buffer for $pH_{25°C}$ = 4.01, phosphate buffer for $pH_{25°C}$ = 7.00, and carbonate buffer for $pH_{25°C}$ = 10.01. At room temperature, the pHs of P2 and B10 are 2.10 and 10.1, respectively. The pHs the of buffer solutions at reaction temperatures were calculated using HCH geochemical modeling software (Shvarov and Bastrakov, 1999) and are listed in Table 3.

Hydrothermal experiments

25 mL polytetrafluoroethylene (PTFE)-lined stainless steel autoclaves were used to conduct the hydrothermal experiments. 15 mL of reaction solution was put into a cell together with 10 mg of krennerite crystal fragments. Hydrothermal experiments (Table 1) were performed over a range of temperatures in electric Muffle furnaces or ovens (both with a temperature regulation precision of ± 2 °C) at 220 °C (runs A1-12 and B1-6), 190 °C (Runs C1-C11) or 160 °C (Runs D1-D11) at autogenous pressures (< 20 bar). For reactions in the presence of air, the amount of O_2 in the system was controlled by the air in the headspace (runs A1- A12). For experiments B1-B6, the headspace of the cell above the solution was filled with Ar in a glove box prior to sealing the autoclave, in order to minimize the amount of O_2(g) in the system. After reaction, the autoclaves were quenched in cold water for 30 minutes and opened. The reacted fluid was collected after the autoclaves were opened, and solids were rinsed three times with Milli-Q water and then three times with acetone before drying. Solution volumes were measured to check for possible leakage. Results from leaking runs were not considered.

Solid-state diffusion (dry runs)

The solid-state transformation experiments (Table 2) were carried out by heating krennerite grains at 220 °C in both unsealed (E1-E3 runs) and sealed evacuated silica glass tubes (F1-F3)

in a Muffle furnace for periods of 24, 168 and 720 hours. Following that, the furnace was turned off and the samples were allowed to cool in the furnace to room temperature.

X-ray Diffraction (XRD)

Room-temperature powder X-ray diffraction (XRD) patterns of the samples were collected on a Huber Guinier Image Plate G670 with $CoK\alpha_1$ radiation (λ = 1.78892 Å). Each sample was ground in an agate mortar using acetone and spread on a Mylar film. Powder diffraction data was collected for 30 min, or recollected for longer periods to obtain a high quality pattern for quantitative phase analysis. The extent of the transformation was determined by the Rietveld quantitative phase analysis method (RQPA) with the aid of the Rietica program (Rietveld 1969; Hunter 1998). Diffraction data in the 2θ range from 20 to 80° were used in the RQPA. A Pseudo-Voigt function with Howard asymmetry (Howard 1982) and Shifted Cheby II function were adopted to model the peak shapes and the background, respectively. Zero shifts were taken from refinements of an external NBS Si standard. For each run, the reaction extent, y, was calculated as $y = 1 - y_{(krennerite)}$, where $y_{(krennerite)}$ is the mole fraction of krennerite among the products as determined by RQPA.

Scanning Electron Microscopy (SEM)

A QUANTA 450 Field Emission Gun Environmental SEM coupled with a TEAM EDS silicon drift energy dispersive spectrometer at Adelaide Microscopy, University of Adelaide, was used for characterization of the morphological and textural features of the grains. The accelerating voltage was maintained at 20 kV. Secondary Electron (SE) imaging was used to characterize the surface morphology of the grains before and after the reaction. For textural studies, samples were embedded in epoxy resin, sectioned, polished with 1 μm diamond paste and evaporatively coated with 15 nm thick carbon films. The polished cross sections were examined in Back Scattered Electron mode and also by reflected light optical microscopy.

Inductively Coupled Plasma Mass Spectrometry (ICP-MS)

An Agilent 7500 Series ICP-MS at Adelaide Microscopy was used to analyze the Au, Ag and Te contents within the solutions. The concentration levels of the calibration solutions were 500, 200, 100, 50, 20, 10 and 0 ppb (blank) of Au, Ag and Te. Depending on their compositions, solutions were either run unprocessed, or were diluted by factors of 100 or 1000 using 2% HNO_3.

Results

Hydrothermal reactions

XRD and SEM examinations confirmed that krennerite has been replaced by Au-Ag alloy under hydrothermal conditions (Figs. 3 and 4). The morphology of the krennerite grains in the starting material is characterized by sharp edges and smooth surfaces. After the reaction, the Au-Ag alloy grains preserved the external dimensions of the primary krennerite grains; in particular, the edges of the grains remained sharp (Figs. 4a-4f). The surface of the grains was highly porous, with pore sizes up to 1500 nm (Figs. 4a and 4c). In cross section the Au-Ag alloy consists of a wormlike filaments, with diameters ranging from 200 to 1000 nm (Figs. 4d-4f). Wire Au-Ag alloy also developed locally (up to 5 μm in diameter, 25 μm in length; Figs. 4b and 4d). As the reaction proceeds, the length of the wire Au-Ag alloy developed to 100 μm and longer (Fig. 4d). From cross-section views, it is clear that the process of replacement initiates at the surface and along cracks within krennerite (Figs. 4e-4f); as the reaction proceeds, the thickness of the Au-Ag alloy rim increases and the krennerite core shrinks, until krennerite is ultimately fully replaced by Au-Ag alloy. The interface between the Au-Ag alloy and krennerite remains sharp during the process. The overall textures and habit of the Au-Ag alloy produced are identical under acidic and basic conditions. The final product Au-Ag alloy is porous, similar to that formed from the replacement of calaverite and sylvanite under similar hydrothermal conditions (Zhao et al.

2009; 2013). The average composition of the product Au-Ag alloy determined by electron probe microanalysis is $Au_{0.85}Ag_{0.15}$ (calculated on the basis of Au + Ag =1) (average 21 points), with an Au range of 0.79 to 0.87. The composition of this Au-Ag alloy is similar to that obtained via the transformation of sylvanite (Zhao et al. 2013).

The results of solution ICP-MS (Table 1) show that most of the Te was lost to the solution. The concentration of aqueous Te increases as the reaction progresses. The Te concentrations were lower under acidic condition (49 to 291 ppm) than under basic condition (171 to 360 ppm), reflecting the lower solubility of Te under acidic conditions (Zhao et al. 2009; Grundler et al. 2013). This result is consistent with reaction rates, which are slower at the lower pH. According to the sample weight and fluid volume used in each experiment, complete dissolution of the krennerite grains would liberate approximately 390 ppm Te, 250 ppm Au and 30 ppm Ag in solution. The ICP-MS results of Te are generally consistent with the Te concentrations calculated from the reaction extents, assuming all Te is in solution (Table 1). In contrast, only small amounts of Au (< 2 ppb) and Ag (<72 ppb) are present in the solution.

Effects of solution pH

Experimental runs exploring the effects of solution pH on the replacement reaction were undertaken by using two solutions at fixed reaction conditions (T = 220 °C, solid to fluid ratio (S/F) = 0.67 g/L, $[Cl^-]$ = 0.01 *m*). Reaction runs were conducted for 2, 4, 6, 12, 24, 48 and 72 hours. The results are summarized in Table 1 and plotted in Figure 5. Under acidic conditions ($pH_{220°C}$ = 3.15, A1-A6), only 69(4)% of krennerite was replaced by Au-Ag alloy after 72 h, while the replacement was completed within 24 h under basic conditions ($pH_{220°C}$ = 8.95, A7-A12).

Oxidant concentration

To study the effect of the oxidant [O_2(aq)] on the reaction extent, a set of experiments was conducted by reducing the amount of available oxygen. For these runs the samples were prepared and loaded in the hydrothermal cell in an Ar-filled glove box (runs B1-B6; Table 1). The results show that the reaction is rather sluggish under both acidic and basic conditions. After 24 h (B6) only 33(2)% of krennerite had been transformed to Au-Ag alloy. This could be compared with the experiment A11, where almost full transformation to Au-Ag alloy was achieved.

Temperature

The effect of temperature on the reaction extent was studied over the temperature range 160 to 220 °C at constant [Cl^-] of 0.01 *m* and S/F of 0.67 g/L. Results are summarized in Table 1 and plotted in Figure 5. Increasing temperature increases the reaction extent. For example, at pH_T ~9 after reacting for 10 h, 88(5)% of the krennerite was replaced at 220 °C (A10), but only 78(4)% at 190 °C (C9) and 53(3)% at 160 °C (D9). After 10 h at pH_T ~ 3, the reaction extents were 35(2)% at 220 °C (A3), 15(1)% at 190 °C (C3) and 9(1)% at 160 °C (D3). The results can be modeled using the Avrami equation (Fig. 6) (e.g., Lasaga 1984; Wang et al. 2005a, b; Zhao et al. 2009). The calculated Avrami time exponents n and rate constants k for each temperature series are summarized in Table 3 and linear regression plotted in Figures 6a-f. The slope of the lines, i.e., the time exponent n, decreases systematically with decreasing temperature (from 1.23 to 1.07 for pH_T ~9 and from 0.65 to 0.55 for pH_T ~2), without noticeable change in the texture of the product. The plot of ln(k) vs. 1/T reveals a systematic behavior consistent with the Arrhenius relationship (Fig. 6h). Linear regression on the data yields an activation energy E_A for the overall replacement reaction of 42 ± 2 kJ/mol, and a pre-exponential factor A of 1.4 ± 1.0 s^{-1}.

Solid-state reactions

Solid-state decomposition experiments were carried out at 220 °C in both unsealed and sealed quartz glass tubes. XRD patterns show that there was no reaction or change in the krennerite crystal fragments detected after 30 days (Table 2). High-resolution SEM images of grain cross-sections show no phase change or cracks. This indicates that, compared with reactions conducted under hydrothermal conditions, the solid-state transformation of krennerite to Au-Ag alloy has not occurred or occurred only at a very slow rate at 220 °C. Whether the sample was heated in air or under vacuum did not affect the progress of any solid-state reaction under dry conditions.

Discussion

Evidence for coupled dissolution re-precipitation reaction

Many pseudomorphic reactions proceed via an ICDR reaction mechanism, where the dissolution of the parent phase is coupled (in time and space) to the precipitation of the product phase at the reaction front (Putnis 2009). The fact that krennerite can be replaced by Au-Ag alloy under hydrothermal conditions, but no reaction is observed when the samples are heated at the same temperature in the absence of a fluid, is convincing evidence that this transformation is primarily a fluid-mediated process. Changes in solution chemistry show that the majority of the Te is eventually lost to the solution over the course of the reaction, but the Au and Ag contents of the solution remain at low levels (<< 1 ppm). This is indicative of krennerite dissolution and rapid precipitation of Au-Ag alloy during the reaction.

The textural features of some of the products (high porosity; sharp reaction fronts without a significant gap between the parent and product phases; lack of evidence for Au/Ag diffusion at the reaction front) are all consistent with an ICDR reaction mechanism (e.g., Putnis and Mezger 2004; Xia et al. 2009a,b; Brugger et al. 2010). The secondary Au-Ag alloy rim

displays nano- and micro-scale porosity. Unlike the filamentous Au-Ag alloy observed in the transformations of calaverite and sylvanite, which have their long axes perpendicular to the surface of the parent telluride (Zhao et al. 2009, 2013), the Au-Ag alloy filaments formed in the replacement of krennerite are much more wire-like and coiled and twisted (Figs. 4c-4d). This structural difference may be a reflection in the underlying topology of the structures: the layer structures of calaverite and sylvanite compared with the more corrugated or zig-zag topology in krennerite. The wire-mesh exhibits a high porosity and facilitates fluid transport to and from the reaction front. Such porosity is a key feature of ICDR reactions, enabling a continuous transport of solutes to and from the reaction interface (Putnis and Putnis 2007; Putnis 2009). In the case of krennerite, the porosity allows influx of oxidant and removal of dissolved Te (see equations (1) and (2)). The sharp reaction front between krennerite and Au-Ag alloy is observed in all runs. In contrast, processes driven by solid-state diffusion are expected to result in structural and chemical gradients (e.g., Watson and Cherniak 1997; Geisler et al. 2003).

The pH dependence of the reaction extent also confirms that the replacement of krennerite by Au-Ag alloy occurs via a coupled dissolution – reprecipitation reaction (Putnis and Mezger 2004; Xia et al. 2009a; Brugger et al. 2010). Higher Te solubility at high pH (Grundler et al. 2013) results in faster krennerite dissolution rates for these solution conditions compared to low pH solution conditions. In cases where krennerite dissolution is the rate-limiting process (see below), this explains the larger reaction extents measured at pH_T ~9 compares to those at pH_T ~3 (Table 1).

Chemical reactions in the replacement process

In order to write chemical reactions for the overall reactions and for the dissolution and precipitation steps, the nature of the predominant aqueous Te, Au, and Ag complexes needs to be assessed. Zhao et al. (2013) built log $f\,O_2$(g) versus pH diagrams to discuss the relative

290 solubilities of Au, Ag and Te at 200 ˚C in a solution containing 0.01 *m* chloride for a system
291 containing amounts of Au, Ag and Te consistent with the amounts present in our experiments.
292 The results show that Te is mainly present as H_2TeO_3(aq) under acidic to slightly basic
293 ($pH_{200°C}$ 2-7) conditions, while $HTeO_3^-$ predominates under more basic conditions. The
294 dominant Ag aqueous species is AgCl(aq) under acidic conditions, but $Ag(OH)_2^-$
295 predominates under basic conditions. Similarly, AuCl(aq) predominates under acidic
296 conditions, and $Au(OH)_2^-$ under basic conditions. Note that Au(OH)(aq) was excluded from
297 the model; when included, this species was predominant even at $pH_{220\,°C}$ 2.9 (Stefánsson and
298 Seward 2003; Usher et al. 2009).

299 Taking O_2(aq) as the oxidant and assuming Au immobility, the overall reaction of krennerite
300 to Au-Ag alloy can be described depending on pH, as:

301 acidic conditions (buffer P2, $pH_{220°C}$ = 3.15):

302 $$Au_{3.28}Ag_{0.72}Te_{8.00} + 8\ O_2\ (aq) + 7.89\ H_2O + 0.23\ H^+\ (aq) + 0.23\ Cl^-$$

303 $$= 3.77\ Au_{0.87}Ag_{0.13}\ (s) + 0.23\ AgCl\ (aq) + 8\ H_2TeO_3\ (aq); \quad (1)$$

304 basic conditions (buffer B10, $pH_{220°C}$ = 8.95):

305 $$Au_{3.28}Ag_{0.72}Te_{8.00} + 8\ O_2\ (aq) + 0.12\ H_2O + 8.23\ OH^-\ (aq)$$

306 $$= 3.77\ Au_{0.87}Ag_{0.13}\ (s) + 0.23\ Ag(OH)_2^-\ (aq) + 8\ HTeO_3^-\ (aq). \quad (2)$$

307 The overall reaction is an oxidation reaction, promoted by lower pH under acidic, and higher
308 pH under basic conditions (see Zhao et al. 2009). Note that reactions (1) and (2) would result
309 in ppm level Ag in solution (1.3 to 9.5 ppm, calculated on the basis of the Te contents
310 measured in Table 1), higher that the Ag levels measured. These calculated Ag contents are
311 below the AgCl(s) solubility at $T \geq 160$ ˚C. At room temperature, however, the calculated

312 solubility of AgCl(s) is 65 ppb under both basic and acid conditions, suggesting that at room
313 temperature, Ag solubility is limited by AgCl(s).

314 **Dissolution of krennerite.** The dissolution of krennerite in the presence of O_2 (aq) can be
315 written depending on pH, as:

316 acidic conditions (buffer P2, $pH_{220°C} = 3.15$):

317 $$Au_{3.28}Ag_{0.72}Te_{8.00} + 9\ O_2\ (aq) + 6\ H_2O + 4\ H^+\ (aq) + 4\ NaCl\ (aq)$$

318 $$= 3.28\ AuCl\ (aq) + 0.72\ AgCl\ (aq) + 4\ Na^+ + 8\ H_2TeO_3\ (aq); \quad (3)$$

319 basic conditions (buffer B10, $pH_{220°C} = 8.95$):

320 $$Au_{3.28}Ag_{0.72}Te_{8.00} + 9\ O_2\ (aq) + 2\ H_2O + 12\ OH^-\ (aq)$$

321 $$= 3.28\ Au(OH)_2^-\ (aq) + 0.72\ Ag(OH)_2^-\ (aq) + 8\ HTeO_3^-\ (aq). \quad (4)$$

322 The oxidation of Te to Te^{4+} is necessary to allow Te to be removed into solution. This is
323 consistent with the ICP-MS results, showing that the majority of the Te is eventually lost to
324 solution over the course of the reaction. The oxidation of Te is confirmed by the fact that the
325 reacted solutions turn bright yellow by adding concentrated HCl in the solution, a coloration
326 due to the formation of Te(IV) chlorocomplexes (Nabivanets and Kapantsyan 1968). Hence,
327 krennerite dissolution in our experiments is an oxidation process, and the availability of
328 oxygen plays an important role in controlling the reaction extent under all conditions, as
329 illustrated by the lower reactions extents obtained in runs where oxygen levels were limited
330 (series B in Table 1).

331 **Precipitation of krennerite to Au-Ag alloy.** The Au-Ag alloy forms via precipitation from
332 aqueous solution, according to the reaction depending on pH:

333 acidic conditions (buffer P2, $pH_{220°C} = 3.15$):

334 $x\ AuCl\ (aq) + (1\text{-}x)\ AgCl\ (aq) + 0.5\ H_2O + Na^+(aq)$

335 $$= Au_xAg_{1-x}(s) + NaCl(aq) + 0.25\ O_2(aq) + H^+\ (aq)\ ; \quad (5)$$

336 basic conditions (buffer B10, $pH_{220°C} = 8.95$):

337 $x\ Au(OH)_2^-\ (aq) + (1\text{-}x)\ Ag(OH)_2^-\ (aq)$

338 $$= Au_xAg_{1-x}\ (s) + 0.5\ H_2O + 0.25\ O_2\ (aq) + OH^-\ (aq). \quad (6)$$

339 Reactions 5 and 6 describe the reduction of Au(I) and Ag(I), controlled by the redox potential
340 of the fluid at the reaction front. The decrease of oxygen activity favors the precipitation of
341 Au-Ag alloy. Oxygen is continuously removed by the oxidation of tellurium, and the soluble
342 oxidation product leaves the reaction front by mass transport in the fluid. The dissolution of
343 krennerite causes the concentration of aqueous Au and Ag complexes at the reaction front to
344 increase. The precipitation of Au-Ag alloy enables the continuing dissolution of krennerite by
345 consuming the aqueous Au and Ag at the reaction front and by releasing O_2(aq) (Eqs. 5 and
346 6). Thus krennerite dissolution and Au-Ag alloy precipitation feed back into each other, and
347 the reaction progresses until all krennerite or all available O_2(aq) (since the overall reaction
348 consumes oxygens; see equations (1) and (2)) is consumed.

349 **Rate-limiting step.** We can identify three critical steps that may control reaction kinetics in
350 ICDR reactions: (i) solutes must be able to reach (e.g., O_2(aq)) and move away from (e.g.,
351 aqueous Te) the reaction front; (ii) krennerite must dissolve (Eq. 3 and 4); and (iii) Au-Ag
352 alloy must precipitate (Eq. 5 and 6). The overall reaction rate is controlled by the slowest step
353 among these three processes. Xia et al. (2009a) showed that to maintain a nm-scale
354 pseudomorphic replacement, the dissolution reaction needs to be rate-limiting relative to the
355 precipitation reaction. For the replacement of krennerite by Au-Ag alloy, this means that the
356 dissolution of a small amount of krennerite results in a fluid boundary layer that is

357 supersaturated with respect to Au-Ag alloy, leading to rapid heterogeneous nucleation and
358 subsequently growth of Au-Ag alloy from this solution layer at places adjacent to the
359 krennerite dissolution sites. This process is likely favored by surface catalytic effects
360 facilitating nucleation. The coupled krennerite dissolution and Au-Ag alloy reprecipitation
361 process results in pseudomorphic replacement, with preservation of textural details at the sub-
362 micrometer length scale. Diffusion of species (Te(IV) complex and O_2(aq)) through the Au-
363 Ag alloy of increasing thickness is fast enough to maintain the dissolution rate throughout the
364 process. These findings are similar to those shown in detail for the transformation of
365 pentlandite to violarite (Tenailleau et al. 2006; Xia et al. 2009a). Thus, krennerite dissolution
366 is the rate-limiting step in the ICDR process.

367 **Reaction kinetics.** For the replacement of krennerite by Au-Ag alloy, the Avrami exponent *n*
368 increases systematically with increasing temperature (Fig. 6c), without a noticeable change in
369 the texture of the product. The Arrhenius activation energies are E_A of 42 ± 2 kJ/mol at
370 $pH_{220°C}$ ~ 8.95 and 74 ± 6 kJ/mol at $pH_{220°C}$ ~ 3.15; the higher activation energy at low pH
371 reflects the slower reaction under acidic conditions. These activation energy values are close
372 to that of 55 ± 6 kJ/mol obtained for the replacement of calaverite at $pH_{220°C}$ 2.95 (Zhao et al.
373 2009). Therefore, the rate of the transformation from krennerite to Au-Ag alloy is comparable
374 to calaverite. In contrast, sylvanite transformation was slower (Zhao et al. 2013). For example,
375 at $pH_{220°C}$ ~9, almost complete transformation of krennerite and calaverite to gold (Au-Ag
376 alloy) was obtained after 24 hours, but only 19% of Au-Ag alloy plus 56% of calaverite-I
377 formed from sylvanite in the same period under similar solution conditions.

378 *Krennerite and calaverite vs. sylvanite*

379 Krennerite, calaverite, and sylvanite all transform to gold (Au-Ag alloy) under hydrothermal
380 conditions. Krennerite and calaverite follow a simple ICDR reaction path and both minerals
381 transform at similar rates. In contrast, the transformation of sylvanite to Au-Ag alloy is more

sluggish, and follows a complex reaction path in which intermediary phases of calaverite with two contrasting chemical compositions are formed. Here, we relate these fundamental differences to aspects of the crystal structures of the three minerals.

The structures of krennerite, calaverite and sylvanite are built upon distorted $(Au,Ag)Te_6$ octahedra (Pertlik 1984a, b; Dye and Smyth 2012; Schutte and deBoer 1988 ; Bindi et al. 2009). The actual structures of calaverite and sylvanite have a complex modulated character and require a 3+1 dimensional description, but the subtleties of such superspace group description are beyond the scope of this paper (see Bindi et al. 2009). In first approximation, calaverite and sylvanite share a layer structure, and sylvanite can be seen as an ordered derivative structure of calaverite, in which Ag and Au atoms occupy different sites with different octahedral distortions. In contrast, krennerite has a 'zig-zag' structure (Fig. 2). Tendeloo et al. (1984) describe the krennerite structure as a commensurate, interface modulated structure, with Ag being preferentially located along the twin interface (red dotted line in Fig. 2).

The differences in reaction paths among calaverite and sylvanite are related to the fact that sylvanite is an ordered, Ag-rich derivative structure of calaverite. Following the dissolution of sylvanite, a Ag-rich, Te-depleted calaverite (calaverite-I) precipitates epitaxially onto the sylvanite surface, given the close structural similarity between the two phases. The chemistry of calaverite-I reflects the high Ag contents of the dissolving sylvanite, i.e. high concentrations of Ag and high Ag:Au ratios in the solution near the dissolving sylvanite. Calaverite-I is metastable, and breaks down via a solid-state reaction into calaverite-(II) and phase-X (Zhao et al. 2013). According to this pathway, Ag controls the natures and texture of the products.

In contrast, no metastable phase nucleates on the surface of calaverite (Zhao et al. 2009), and calaverite transforms directly into Au-Ag alloy. Although krennerite has a higher Ag content than calaverite, and its dissolution could favor precipitation of a metastable Ag-rich calaverite, this is not observed, and krennerite transforms directly into Au-Ag alloy. This can be explained by the differences in crystal structures of krennerite and calaverite. The absence of continuous planes with calaverite-like topology in krennerite prevents epitaxial nucleation and growth of calaverite on the krennerite surface.

Applications and implications for reactions under hydrothermal conditions

The nature of the krennerite transformation has implications for the treatment of telluride Au ores and for understanding the origin of some unusual telluride assemblages in Nature. At 220 °C, solid-state replacement of krennerite by Au-Ag alloy is slow (months), but krennerite grains ~100 μm in size can be nearly fully replaced in 24 hours in the presence of water, providing a possible alternative to roasting as a pre-treatment of telluride-rich Au ores (Spry et al. 2004; Zhao et al. 2010). This alternative pre-treatment can be applied to all the three major Au-Ag-tellurides.

In this paper we are concerned with the effects of Ag in the Au-Ag tellurides on the mechanism of the transformation of ICDR reactions. The fundamental difference observed for the hydrothermal replacement of calaverite and krennerite (simple ICDR reactions leading to pseudomorphic replacement by gold/Au-Ag alloy) and sylvanite (complex interplay between ICDR and solid-state reactions) can be related to the different crystal structures and the different amount of Ag in the Au-Ag-tellurides. This further illustrates the importance of surface nucleation processes in controlling the outcomes (textures and mineral assemblages) of mineral replacement reactions. Similar processes were described by Qian et al. (2010, 2011) for the sulfidation of magnetite and pyrrhotite.

Acknowledgement

We thank Len Green, Aoife McFadden, and Angus Netting from Adelaide Microscopy Center for their assistance in using the QUANTA 450 SEM, ICP-MS, and electron microprobe. The paper benefitted from careful reviews by L. Bindi and an anonymous reviewer. This work has been made possible by the financial support of the Australian Research Council (Grants DP0880884 and DP1095069).

Reference

Ahmad, M., Solomon, M., and Walshe, J.L. (1987) Mineralogical and geochemical studies of the Emperor gold telluride deposit, Fiji. Economic Geology, 82, 234-270.

Bindi, L., Arakcheeva, A., and Chapuis, G. (2009) The role of silver on the stabilization of the incommensurately modulated structure in calaverite, $AuTe_2$. American Mineralogist, 94, 728-736.

Brugger, J., Etschmann, B., Grundler, P., Liu, W., Testemale, D. and Pring, A. (2012). XAS evidence for the stability of polytellurides in hydrothermal fluids up to 599 ˚C, 800 bar. American Mineralogist, 97, 1519-1522.

Brugger, J., McFadden, A., Lenehan, C.E., Etschmann, B., Xia, F., Zhao, J., and Pring, A. (2010) A Novel route for the synthesis of mesoporous and low-thermal stability materials by coupled dissolution-reprecipitation reactions: mimicking hydrothermal mineral formation. Chimia, 64, 693-698.

Cabri, L.J. (1965) Phase relations in the Au-Ag-Te system and their mineralogical significance. Economic Geology, 60, 1569-1605.

Cook, N.J., Ciobanu, C.L., Spry, P.G., and Voudouris, P. (2009) Understanding gold-(silver)-telluride-(selenide) mineral deposits. Episodes, 32, 249-263.

452 Dye, M.D., and Smyth, J.R. (2012) The crystal structure and genesis of krennerite, Au_3AgTe_8.
453 The Canadian Mineralogist, 50, 119-127.

454 Geisler, T., Pidgeon, R.T., Kurtz, R., Bronswijk, W.V., and Schleicher H. (2003)
455 Experimental hydrothermal alteration of partially metamict zircon. American Mineralogist,
456 88, 1496-1513.

457 Grundler, P., Brugger, J., Etschmann, B., Helm, L., Liu, W., Spry, Paul G., Tian, Y.,
458 Testemale, D., and Pring, A. (2013) Speciation of aqueous tellurium(IV) in hydrothermal
459 solutions and vapors and the role of oxidized tellurium species in gold metallogenesis.
460 Geochimica et Cosmochimica Acta (in press).

461 Howard, C. (1982) The approximation of asymmetric neutron powder diffraction peaks by
462 sums of Gaussians. Journal of Applied Crystallography, 15, 615-620.

463 Hunter, B.A. (1998) Rietica—A visual Rietveld program. International Union of
464 Crystallography Commission on Powder Diffraction Newsletter, 20, 21-23.

465 Lasaga, A.C. (1984) Chemical kinetics of water-rock interactions. Journal of Geophysical
466 Research, 89, 4009-4025.

467 Nabivanets, B.I., and Kapantsyan, E.E. (1968) The tellurium(IV) state in HCl and LiCl
468 solutions. Russian Journal of Inorganic Chemistry, 13, 946-949.

469 Pertlik, F. (1984a) Kristallchemie natürlicher Telluride I: Verfeinerung der Kristallstruktur
470 des Sylvanits; $AuAgTe_4$. Tschermaks Mineralogische und Petrographische Mitteilungen, 33,
471 203-212 (in German).

Pertlik, F. (1984b) Crystal chemistry of natural tellurides II: Redetermination of the crystal structure of krennerite. Tschermaks Mineralogische und Petrographische Mitteilungen 33, 253-262.

Putnis, A. (2009) Mineral Replacement Reactions. Reviews in Mineralogy and Geochemistry, 70, 87-124.

Putnis, A., and Putnis, C.V. (2007) The mechanism of reequilibration of solids in the presence of a fluid phase. Journal of Solid State Chemistry, 180, 1783-1786.

Putnis, C.V. and Mezger, K. (2004) A mechanism of mineral replacement: isotope tracing in the model system KCl-KBr-H_2O. Geochimica et Cosmochimica Acta, 68, 2839-2848.

Qian, G. Xia, F., Brugger, J., Skinner, W.M., Bei, J., Chen, G. and Pring, A. (2011) Replacement of pyrrhotite by pyrite and marcasite under hydrothermal conditions up to 220 ˚C: an experimental study of reaction textures and mechanisms. American Mineralogist, 96, 1878-1893. 36.

Qian, G., Brugger, J., Skinner, W.M., Chen, G. and Pring, A. (2010) An experimental study of the mechanism of the replacement of magnetite by pyrite up to 300 ˚C. Geochimica et Cosmochimica Acta, 74, 5610-5630.

Rietveld, H. (1969) A profile refinement method for nuclear and magnetic structures. Journal of Applied Crystallography, 2, 65-71.

Schutte, W.J., and de Boer, J.L. (1988) Valence fluctuations in the incommensuratly modulated structure of Calaverite ($AuTe_2$). Acta Crystallographica B, 44, 486–494.

Shackleton, J.M., and Spry, P.G. (2003) Telluride mineralogy of the Golden Mile deposit, Kalgoorlie, Western Australia. Canadian Mineralogist, 41, 1503-1524.

494 Shvarov, Y. and Bastrakov, E., 1999. HCh: a software package for geochemical modelling.
495 User's guide. AGSO record 1999/25, 60 pp.

496 Spry, P.G., Chryssoulis, S., and Ryan, C.G. (2004) Process mineralogy of gold: gold from
497 telluride-bearing ores. Journal of the Minerals, Metals and Materials Society, 56, 60-62.

498 Stefánsson, A., and Seward, T. M. (2003) The hydrolysis of gold(I) in aqueous solutions to
499 600°C and 1500 bar. Geochimica et Cosmochimica Acta, 67, 1677-1688.

500 Tenailleau, C., Pring, A., Etschmann, B., Brugger, J., and Studer, A. (2006) Transformation
501 of pentlandite to violarite under mild hydrothermal conditions. American Mineralogist, 91,
502 706-709.

503 Tendeloo, G. Van., Amelinckk, S., and Gregoriades, P. (1984) Electron Microscopic Studies
504 of Modulated Structures in (Au,Ag)Te_2 III. Krennerite. Journal of Solid State Chemistry, 53,
505 281-289.

506 Tunell, G., and Murata, K.J. (1950). The atomic arrangement and chemical composition of
507 krennerite. American Mineralogist, 35, 959-984.

508 Usher A., McPhail, D.C. and Brugger, J. (2009) A spectrophotometric study of aqueous
509 Au(III)-halide-hydroxy complexes at 25˚C. Geochimica et Cosmochimica Acta, 73, 3359-
510 3380.

511 Wang, H., Pring, A., Ngothai, Y., and O'Neill, B. (2005a) A low-temperature kinetic study of
512 the exsolution of pentlandite from the monosulfide solid solution using a refined Avrami
513 method. Geochimica et Cosmochimica Acta, 69, 415-425.

514 Wang, H., Pring, A., Xia, Y., Ngothai, Y., and O'Neill, B. (2005b) Phase evolution and
515 kinetics of the oxidation of monosulfide solid solution under isothermal conditions.
516 Thermochimica Acta, 427, 13-25.

517 Watson, E.B., and Cherniak, D.J. (1997) Oxygen diffusion in zircon. Earth and Planetary
518 Science Letters, 148(3–4), 527-544.

519 Xia, F., Brugger, J., Chen, G., Ngothai, Y., O'Neill, B., Putnis, A., and Pring, A. (2009a)
520 Mechanism and kinetics of pseudomorphic mineral replacement reactions: A case study of
521 the replacement of pentlandite by violarite. Geochimica et Cosmochimica Acta, 73, 1945-
522 1969

523 Xia, F., Brugger J. and Pring, A. (2009b) Three dimensional ordered arrays of zeolite
524 nanocrystals with uniform size and orientation by a pseudomorphic coupled dissolution-
525 reprecipitation replacement route. Crystal Growth & Design, 9, 4902-4906.

526 Zhao, J., Brugger, J., Grundler, P.V., Xia, F., Chen, G., and Pring, A. (2009) Mechanism and
527 kinetics of a mineral transformation under hydrothermal conditions: Calaverite to metallic
528 gold. American Mineralogist, 94, 1541-1555.

529 Zhao, J., Brugger, J., Xia, F., Nogthai, Y., Chen, G., and Pring, A. (2013) Dissolution-
530 reprecipitation versus solid-state diffusion: mechanism of mineral transformations in
531 sylvanite, $(AuAg)_2Te_4$, under hydrothermal conditions. American Mineralogist, 98, 19-32.

532 Zhao, J., Xia, F., Pring, A., Brugger, J., Grundler, P.V., and Chen, G. (2010) A novel
533 pretreatment of calaverite by hydrothermal mineral replacement reactions. Minerals
534 Engineering, 23, 451-453.

535

536 **Tables and Figures**

537

538 Table 1. Summary of the hydrothermal reactions conditions and results*

Run No.	T/(°C)	Reaction Solution#	Time (h)	Rxn. extent (mole %)§	Concentrations of Au, Ag and Te ‡			Te_{calc} (ppm; from reaction extent) ‖
					Ag(ppb)	Au(ppb)	Te(ppm)	
A1	220	P2	4	12(1)	63	0.1	49	49
A2	220	P2	6	33(2)	71	0.2	104	129
A3	220	P2	10	35(2)	4	<0.04	108	136
A4	220	P2	24	60(3)	57	<0.04	147	236
A5	220	P2	48	61(3)	54	1.3	148	239
A6	220	P2	72	69(4)	56	<0.04	291	269
A7	220	B10	2	27(1)	<0.07	<0.04	120	104
A8	220	B10	4	44(2)	<0.07	0.10	216	172
A9	220	B10	6	74(4)	2.8	0.3	310	287
A10	220	B10	10	88(5)	8.8	0.1	330	341
A11	220	B10	24	99(5)	<0.07	0.3	360	386
A12	220	B10	48	100(5)	<0.07	0.1	319	390
B1†	220	P2	4	6(1)	--	--	--	--
B2†	220	P2	6	8(1)	--	--	--	--
B3†	220	P2	24	12(1)	--	--	--	--
B4†	220	B10	4	20(1)	--	--	--	--
B5†	220	B10	6	28(1)	--	--	--	--
B6†	220	B10	24	33(2)	--	--	--	--
C1	190	P2	4	8(1)	--	--	--	--
C2	190	P2	6	11(1)	--	--	--	--
C3	190	P2	10	15(1)	--	--	--	--
C4	190	P2	24	29(2)	--	--	--	--
C5	190	P2	48	38(2)	--	--	--	--
C6	190	P2	120	41(2)	--	--	--	--
C7	190	B10	4	24(1)	--	--	--	--
C8	190	B10	6	38(2)	--	--	--	--
C9	190	B10	10	78(4)	--	--	--	--

C10	190	B10	24	91(5)	--	--	--	--
C11	190	B10	48	99(5)	--	--	--	--
D1	160	P2	4	5(1)	--	--	--	--
D2	160	P2	6	7(1)	--	--	--	--
D3	160	P2	10	9(1)	--	--	--	--
D4	160	P2	24	14(1)	--	--	--	--
D5	160	P2	48	27(1)	--	--	--	--
D6	160	P2	120	30(2)	--	--	--	--
D7	160	B10	4	13(1)	--	--	--	--
D8	160	B10	6	16(1)	--	--	--	--
D9	160	B10	10	53(3)	--	--	--	--
D10	160	B10	24	68(3)	--	--	--	--
D11	160	B10	48	85(4)	--	--	--	--

* The ratio between the weight of krennerite and the volume of fluid is 0.67.

"P" phosphate buffer solution, "B" borate buffer solution.

§ Obtained from powder X-ray diffraction patterns by Rietveld quantitative phase analysis.

‡ Obtained from ICP-MS by the analysis of Au, Ag and Te concentrations in the reacted solution samples. The detection limit for Au, Ag and Te are 0.04 ppb, 0.07 ppb and 0.2 ppm, respectively. The concentration would be Au (242-259ppm), Ag (29-32 ppm) and Te (388-400 ppm), if the 10mg (±0.5) of krennerite is all dissolved in the solution.

|| Amount of aqueous Te calculated based on the reaction extent assuming that all the Te remains in solution.

†Autoclaves were filled with Ar before sealing.

539

540

Table 2. The solid-state transformation experiments by heating krennerite grains at 220℃ in both unsealed and sealed evacuated quartz glass tubes

Run No.	T/(℃)	Time/(days)	Air conditions	Results
E1	220	1	Air	No reaction
E2	220	7	Air	No reaction
E3	220	30	Air	No reaction
F1	220	1	Vacuum	No reaction
F2	220	7	Vacuum	No reaction
F3	220	30	Vacuum	No reaction

Table 3. Calculated time exponent n and rate constant k, as a function of temperature (T) and pH

T (℃)	pH_T	Buffer	n		$k\times10^{-5}$ (s^{-1})		R^2
220	3.15	P2	0.65	±0.14	0.64	±1.52	0.895
190	2.94	P2	0.58	±0.08	0.12	±0.84	0.921
160	2.75	P2	0.55	±0.05	0.051	±0.58	0.962
220	8.95	B10	1.23	±0.15	5.2	±1.43	0.959
190	8.94	B10	1.18	±0.15	2.7	±1.60	0.939
160	8.97	B10	1.07	±0.20	1.3	±2.14	0.875

550 **Figure captions**

551 Figure 1. Compositions and reactivity of Au-Ag-tellurides under hydrothermal conditions.
552 Modified after Zhao et al. (2013).
553

554 Figure 2. Projections of the crystal structures of, and major reaction paths for the replacement
555 of sylvanite, calaverite and krennerite. Crystal structure data from Dye and Smyth (2012) for
556 krennerite; Pertlik (1984a) for sylvanite; and Bindi et al. (2009) for calaverite.
557

558 Figure 3. Power X-ray diffraction traces illustrating the progress of the hydrothermal reaction.
559 (a) Unreacted krennerite; (b) partially reacted grains after 4 hours (sample NO. A8);
560 (c) totally reacted grains after 24 hours (A11). The black dots are the observed patterns; the
561 red lines through the dark crosses are the calculated patterns; the green lines at the bottom are
562 the difference between observed and calculated patterns.
563

564 Figure 4. Secondary electron images showing reaction textures from hydrothermal reactions.
565 **(a)** Sharp edges of the reacted grain, showing the preservation of the external dimensions of
566 the primary krennerite grains (sample NO. A7). **(b)** Rough surface of the 24-hour reacted
567 grain (A11), showing an overgrowth of a porous Au-Ag alloy layer. **(c)** The surface of the
568 reacted grain (A12), showing the textures of the Au-Ag alloy and associated porosity. **(d)** The
569 internal structure of highly porous Au- Ag alloy (A12), showing filament-shaped Au-Ag
570 alloy crystals. **(e)** Back-scattered electron images of cross-section of partially reacted grains
571 (A2), showing the reaction proceeding down cracks within the krennerite crystal fragments.
572 **(f)** Boundary between the parent and daughter crystal of run A6, showing larger Au-Ag alloy
573 particles coexisting with fine-grained Au-Ag alloy in the resulted gold rim.

574

575 Figure 5. Plots of reaction extent versus reaction time at different reaction pHs and
576 temperatures. To take into account the errors from both sample preparation and the Rietveld
577 fit, the error on the phase proportion is estimated to 5% on each determination.

578

579 Figure 6. Kinetics of the replacement of krennerite by Au-Ag alloy at different pHs and
580 temperatures [for all solutions: (Cl^-) = 0.01 m, S/F = 0.67 g/L]. **(a–f)** Avrami plots showing
581 the linear regression (fit parameters listed in Table 3) for the different runs at different pHs
582 and different temperatures; t is in seconds. Error bars correspond to a 5% on the reaction
583 extent y are shown when errors are larger than the symbols. **(g)** Avrami time exponent n
584 plotted as a function of temperature, for reactions in buffer B10. **(h)** Arrhenius plot of the
585 Avrami reaction rate constant k (s^{-1}) as a function of temperature, for reactions in buffer B10.

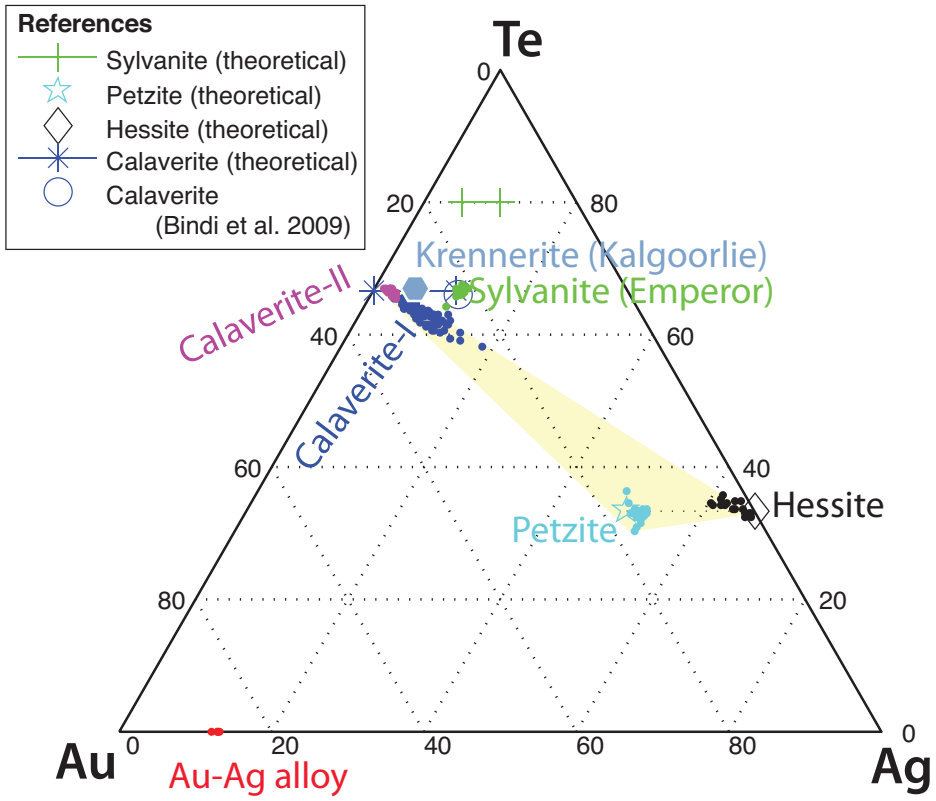
References
Sylvanite (theoretical)
Petzite (theoretical)
Hessite (theoretical)
Calaverite (theoretical)
Calaverite
(Bindi et al. 2009)
Te
Au
Ag
0
20
40
60
80
Krennerite (Kalgoorlie)
Sylvanite (Emperor)
Calaverite-II
Calaverite-I
Petzite
Hessite
Au-Ag alloy

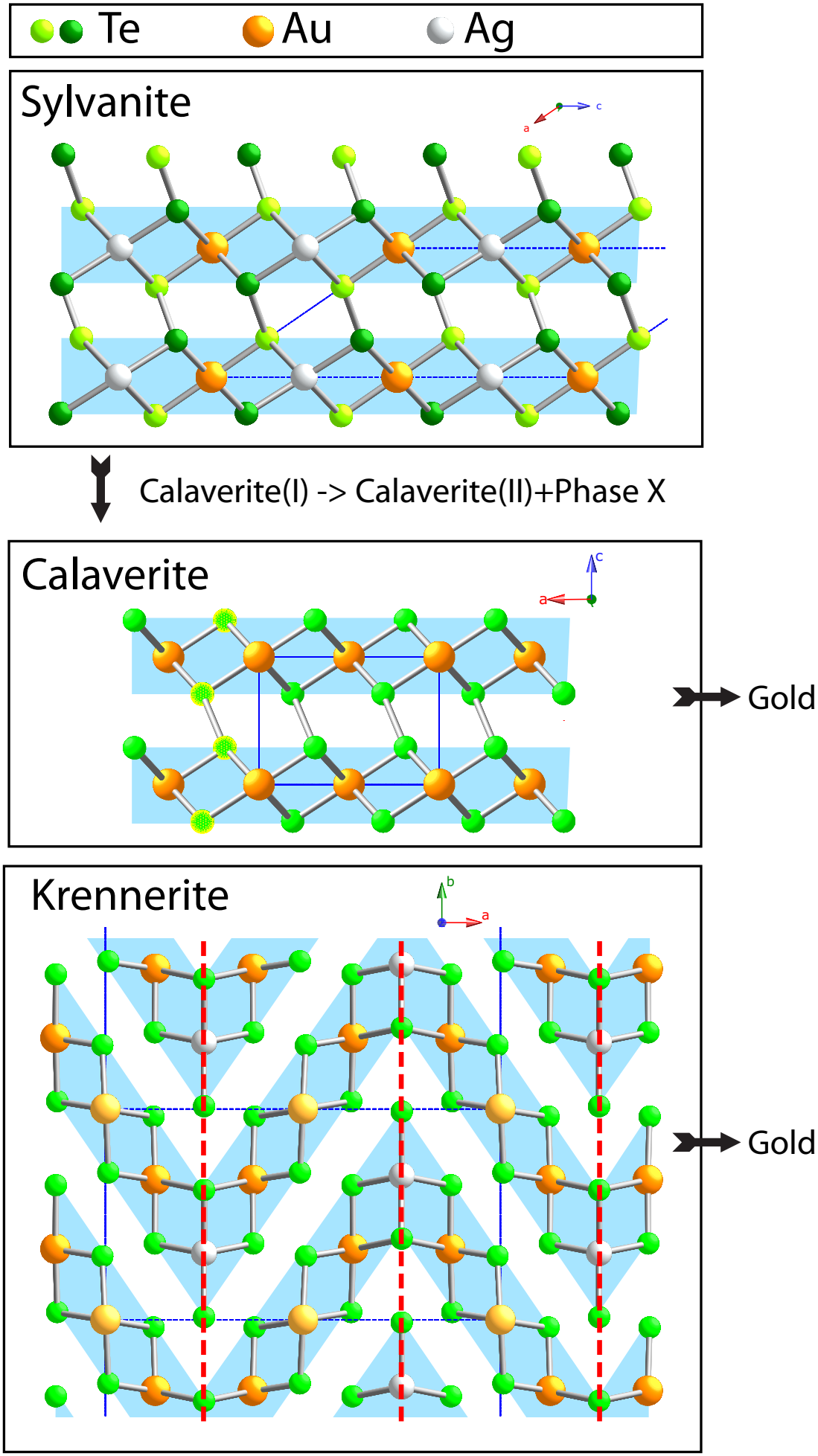
Te
Au
Ag
Sylvanite
c
a
Calaverite(I) -> Calaverite(II)+Phase X
Calaverite
c
a
Gold
Krennerite
b
a
Gold

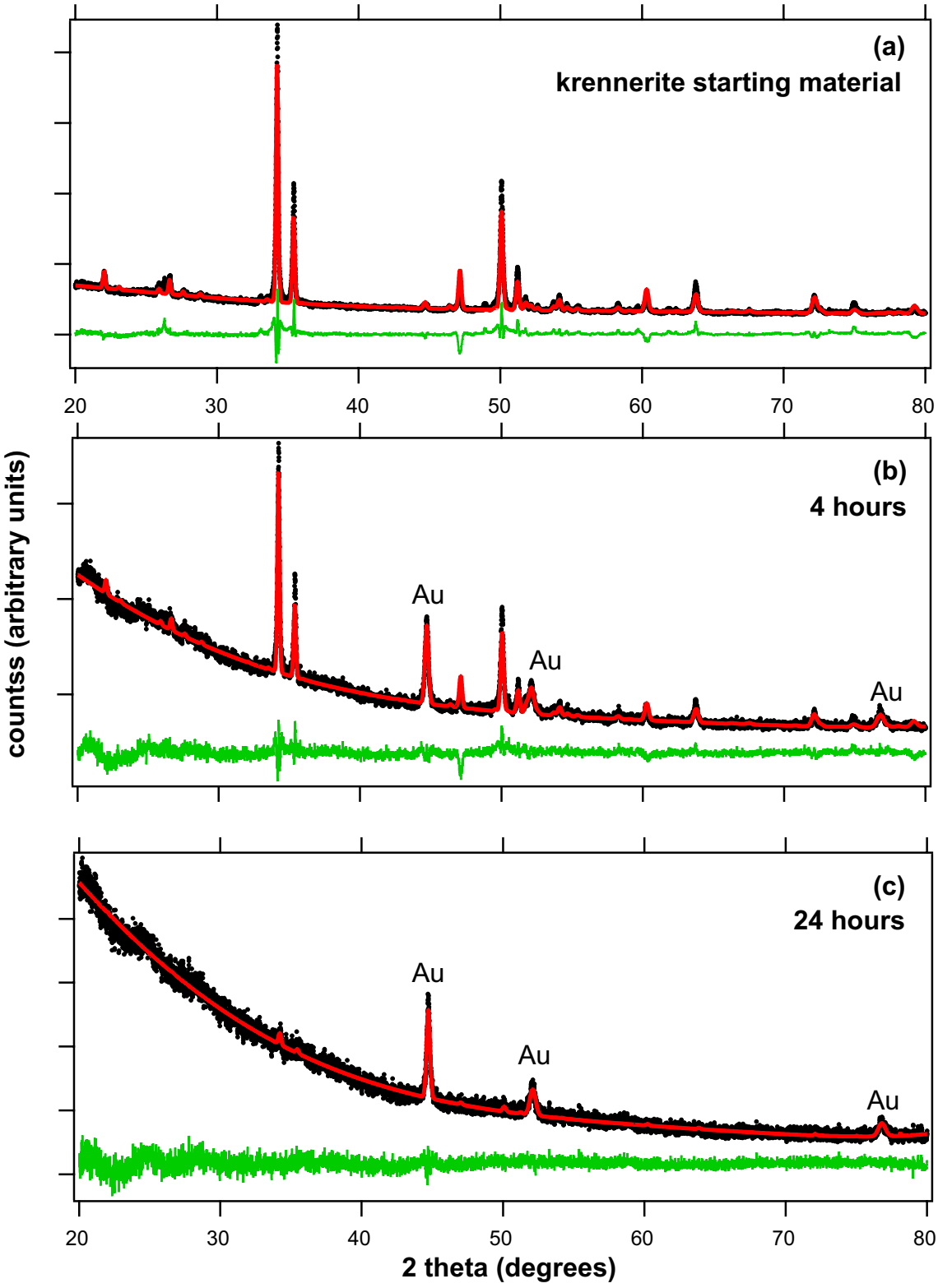
(a)
krennerite starting material
(b)
4 hours
Au
Au
Au
(c)
24 hours
Au
Au
Au
countss (arbitrary units)
20
30
40
50
60
70
80
2 theta (degrees)

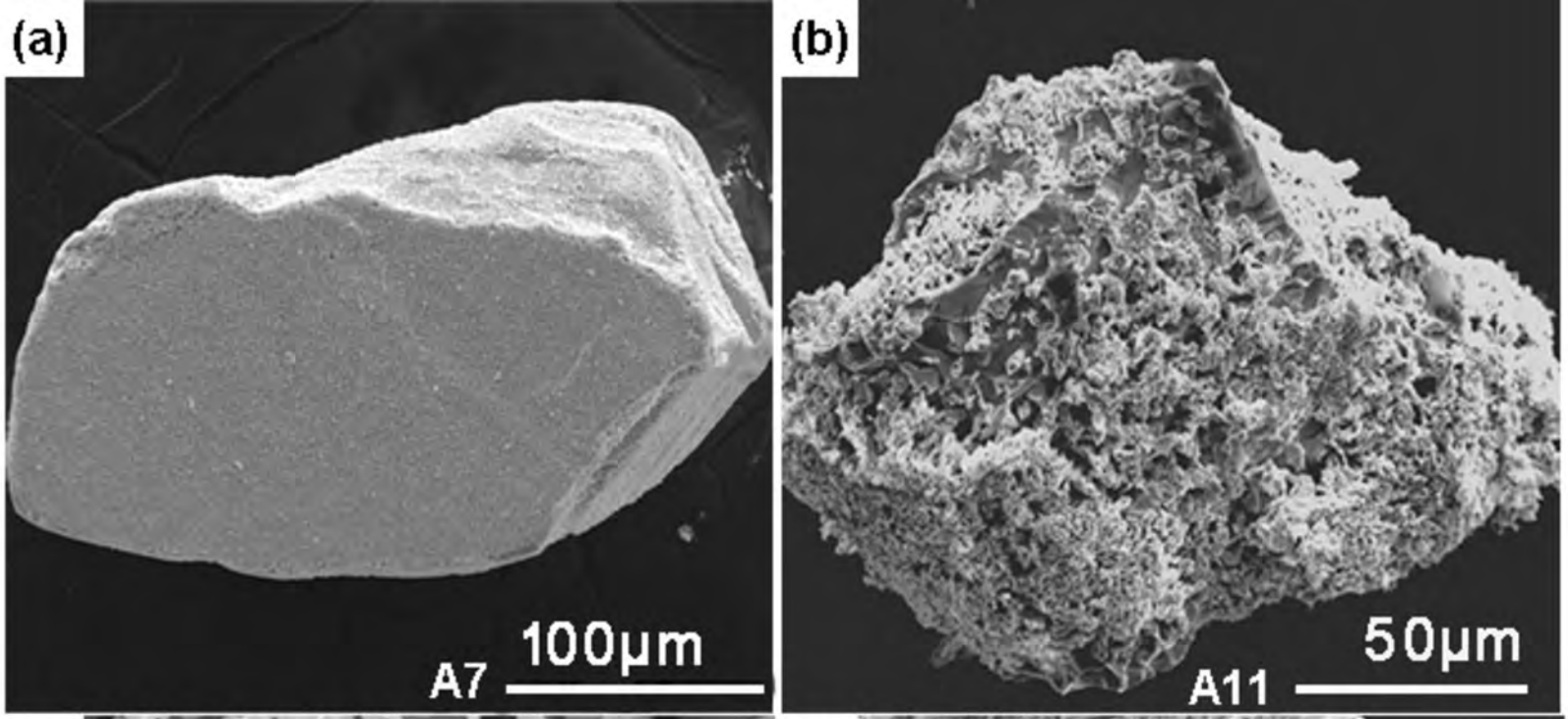
(a)
A7
100μm
(b)
A11
50μm

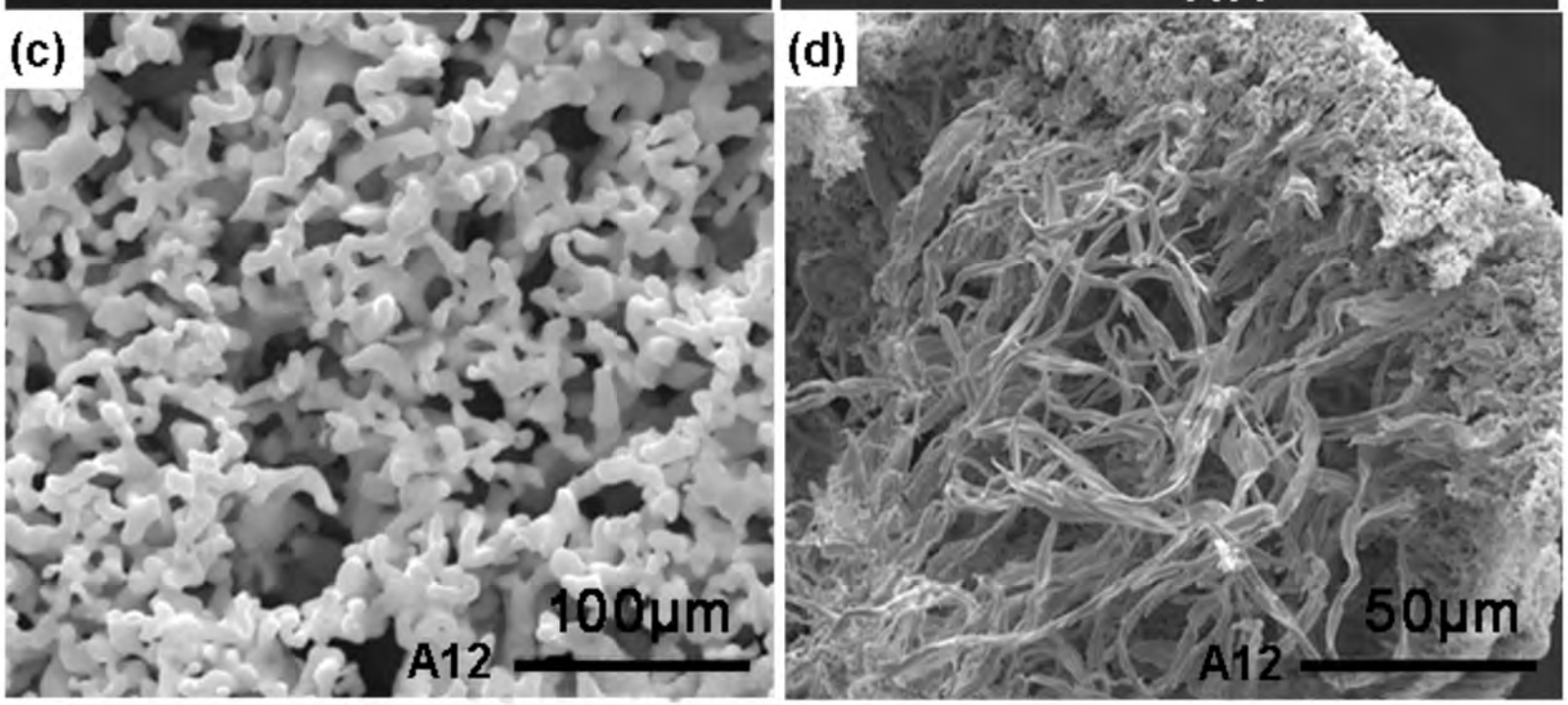
(c)
A12
100μm
(d)
A12
50μm

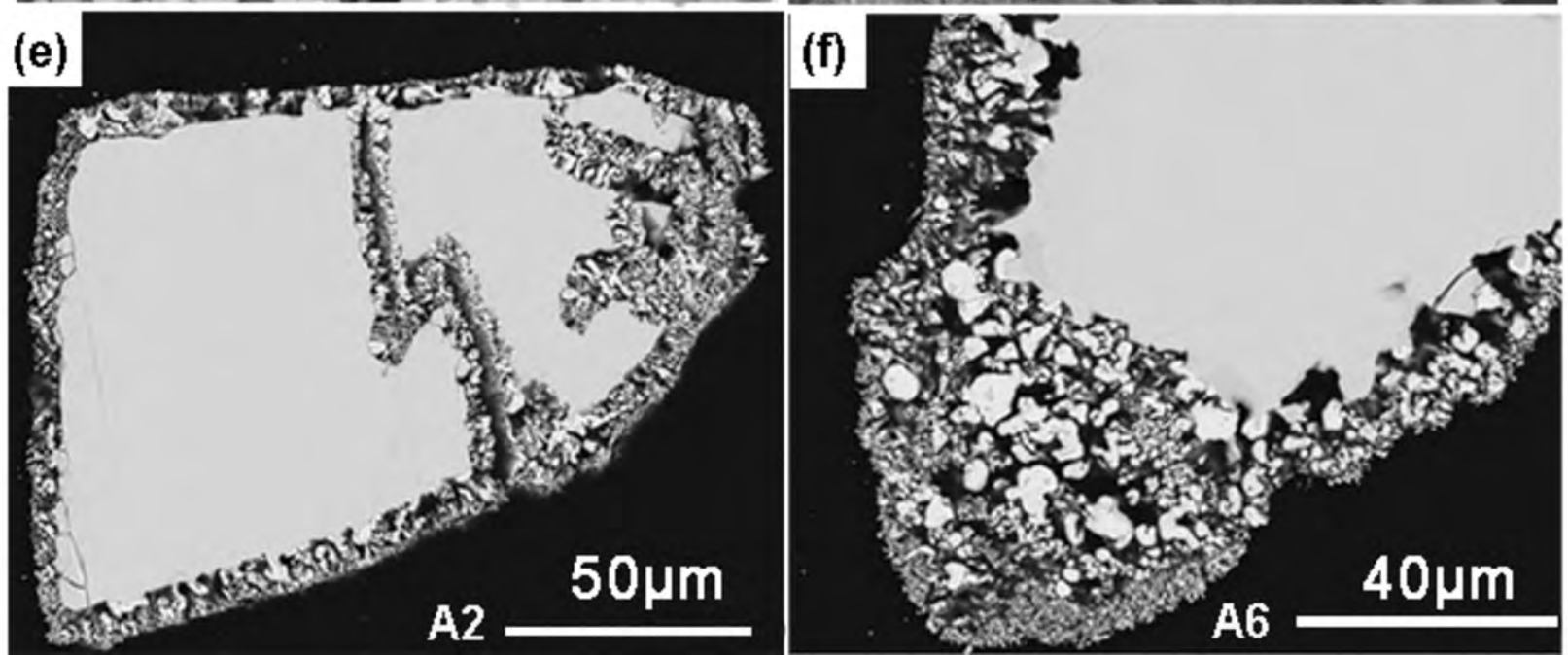
(e)
A2
50μm
(f)
A6
40μm

(a)
T=220°C
Buffer P2
(b)
T=220°C
Buffer B10
(c)
T=190°C
Buffer P2
(d)
T=190°C
Buffer B10
(e)
T=160°C
Buffer P2
(f)
T=160°C
Buffer B10
reaction extent(%)
time(h)

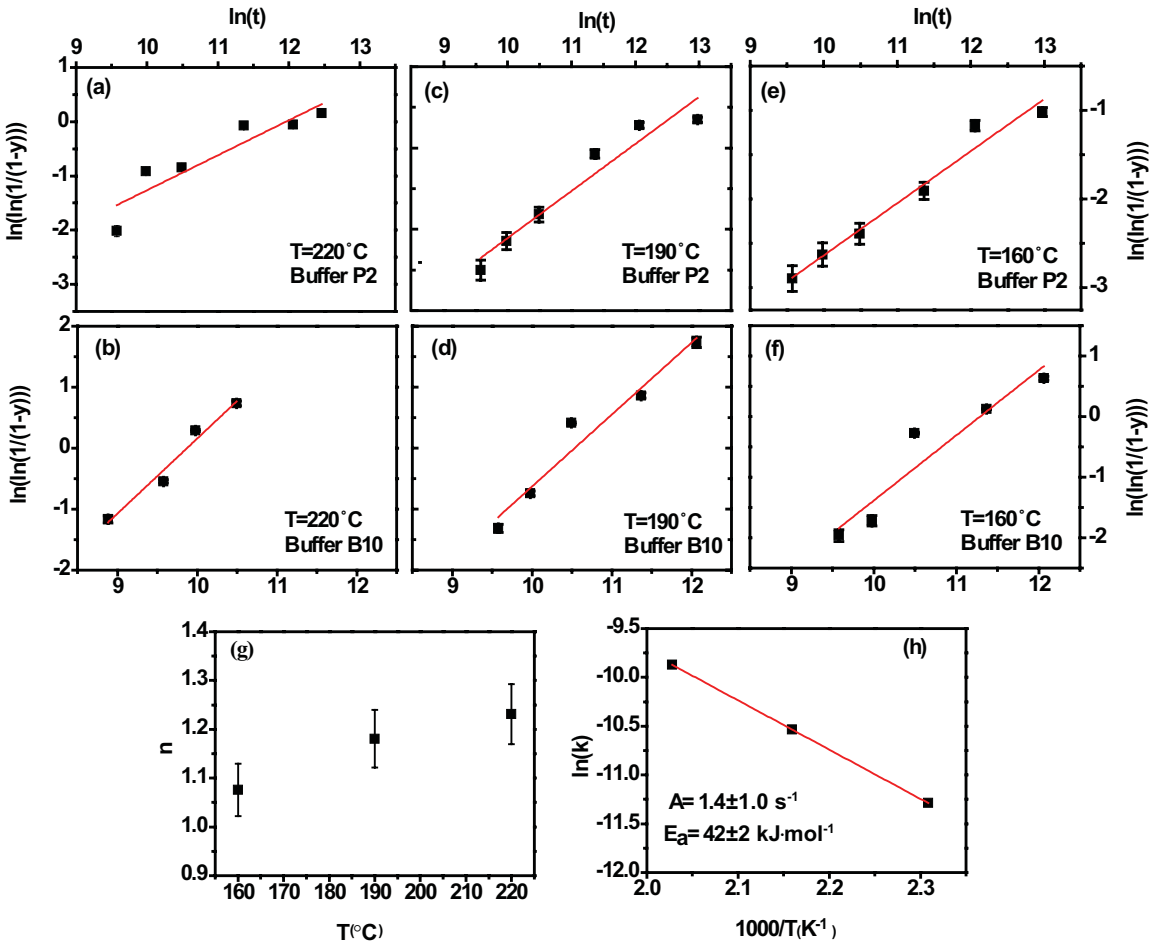
(a)
T=220˚C
Buffer P2
(c)
T=190˚C
Buffer P2
(e)
T=160˚C
Buffer P2
(b)
T=220˚C
Buffer B10
(d)
T=190˚C
Buffer B10
(f)
T=160˚C
Buffer B10
ln(t)
ln(ln(1/(1-y)))
(g)
n
T(°C)
(h)
ln(k)
A= 1.4±1.0 s-1
Ea= 42±2 kJ·mol-1
1000/T(K-1)